made on either side of the epithelium. The control Ringer contained 113 mM NaCl, 26 mM $NaHCO_3$, 5.6 mM glucose, 5 mM KCl, 0.8 mM $MgCl_2$, 1.8 mM $CaCl_2$, and 1.0 mM NaH_2PO_4 and was bubbled with 95% O_2–5% CO_2 to pH 7.4.
9. G. M. Loughlin, G. A. Gerencer, M. A. Crowder, R. L. Boyd, J. A. Mangos, *Experientia* **38**, 1451 (1982).
10. J. Durand, W. Durand-Arczynska, P. Haab, *Pfluegers Arch.* **392**, 40 (1981).
11. M. J. Welsh, J. H. Widdicombe, J. A. Nadel, *J. Appl. Physiol.* **49**, 905 (1980).
12. I. T. Nathanson, J. H. Widdicombe, J. A. Nadel, *ibid.* **55**, 1257 (1983).
13. J. J. Smith and M. J. Welsh, *J. Clin. Invest.* **91**, 1590 (1993). They added 100 μl of culture medium to the mucosal side of the monolayer, covered it with mineral oil to prevent evaporation, and measured the volume of fluid remaining after 24 hours. Unstimulated cultures absorbed fluid, but the J_v rates were 1/10 to 1/50 of those reported here. During the 24-hour sampling period, large pH and electrolyte gradients developed that could have altered active ion and fluid transport. In our experiments, J_v and bioelectric properties were continuously measured in symmetrical solutions with a time resolution of ≤1 min.
14. D. J. Benos, *Am. J. Physiol.* **242**, C131 (1982).
15. In 20 HNE monolayers from 11 normal individuals, the means (± SEM) of baseline J_v, *TEP*, and R_t were 2.3 ± 0.3 μl cm^{-2} $hour^{-1}$, −24.8 ± 7.8 mV, and 1072 ± 259 ohm · cm^2, respectively. In 14 of these monolayers (eight individuals), amiloride decreased J_v and *TEP* to 0.3 ± 0.2 μl cm^{-2} $hour^{-1}$ and −3.9 ± 1.4 mV, respectively, and increased R_t to 1651 ± 329 ohm · cm^2 (steady-state); all the changes are significant ($P < 0.01$ or 0.05, unpaired Student's *t* test). In six of the amiloride-treated monolayers (four individuals), the mixture of CPT-cAMP and IBMX significantly ($P < 0.01$) reduced J_v and R_t. The peak values were −1.4 ± 0.4 μl cm^{-2} $hour^{-1}$ and 781 ± 44 ohm · cm^2; *TEP* increased to −25.3 ± 8.2 mV; J_v then returned to a steady-state level of −0.4 ± 0.3 μl cm^{-2} $hour^{-1}$. In six other amiloride-treated monolayers (four individuals), ATP significantly ($P < 0.01$) reduced J_v and R_t. The peak values were −2.9 ± 0.5 μl cm^{-2} $hour^{-1}$ and 618 ± 183 ohm · cm^2. *TEP* increased to −20.3 ± 1.7 mV and J_v was −0.6 ± 0.2 μl cm^{-2} $hour^{-1}$ in the steady state.
16. N. J. Willumsen and R. C. Boucher, *Am. J. Physiol.* **256**, C226 (1989).
17. M. P. Anderson and M. J. Welsh, *Proc. Natl. Acad. Sci. U.S.A.* **88**, 6003 (1991).
18. M. R. Knowles, L. L. Clarke, R. C. Boucher, *N. Engl. J. Med.* **325**, 533 (1991).
19. S. J. Mason, A. M. Paradiso, R. C. Boucher, *Br. J. Pharmacol.* **103**, 1649 (1991); L. L. Clark and R. C. Boucher, *Am. J. Physiol.* **263**, C348 (1992); H. A. Brown, E. R. Lazarowski, R. C. Boucher, T. K. Harden, *Mol. Pharmacol.* **40**, 648 (1991). These studies suggest that ATP or UTP activates a putative 5′-nucleotide receptor, which is linked to Cl^- secretion by inositol phosphate production and mobilization of Ca^{2+} from intracellular stores.
20. In the absence of amiloride, CPT-cAMP and IBMX (100 μM each) either increased, decreased, or had little effect on J_v, *TEP*, and R_t in normal HNE cultures ($n = 5$). These responses are not due to variations among cultures because all of the cultures from these individuals showed secretory responses to CPT-cAMP plus IBMX in the presence of amiloride. The effect of cAMP on J_v may be determined by the balance of its effects on Na^+ absorption and Cl^- secretion (*1–3, 13*). In cultures from normal individuals and patients with CF, apical addition of UTP (100 μM) reduced J_v, increased *TEP*, and decreased R_t. In three (two normal, one CF) of the seven cultures examined, J_v was actually reversed from absorption to a small transient secretion in response to UTP; in the other four cultures (two normal, two CF) absorption was reduced.
21. Nasal polyps were obtained from four CF patients (all males; mean age, 10 ± 2 years) and genotyped as follows: three ΔF508/ΔF508 and one ΔF508/R560T. Both mutations are associated with a severe phenotype [B. Kerem *et al.*, *Proc. Natl. Acad. Sci. U.S.A.* **87**, 8447 (1990)].
22. C. Jiang and S. S. Miller, unpublished data.
23. Tracheas were obtained from three CF patients (two males, one female; mean age, 33 ± 4 years) and were genotyped as follows: one ΔF508/ΔF508, one ΔF508/unknown, and one ΔF508/R560T.
24. N. Bradbury *et al.*, *Science* **256**, 530 (1992).
25. M. Yamaya, T. Ohrui, W. E. Finkbeiner, J. H. Widdicombe, *Am. J. Physiol.* **265**, L170 (1993).
26. We thank J. Carlson and L. Zlock for technical assistance and J. P. Johnston and E. Louie (Children's Hospital Oakland Research Institute) for genotyping the samples. Supported by Cystic Fibrosis Research, Inc. (S.S.M.), Tobacco-Related Disease Research Program, State of California (1RT 443) (S.S.M.), and NIH (HL 42368) (W.E.F. and J.H.W.).

4 June 1993; accepted 23 August 1993

Structure-Function Analysis of the Ion Channel Selectivity Filter in Human Annexin V

Robert Berendes, Dieter Voges, Pascal Demange, Robert Huber,* Alexander Burger

Electrophysiology and structural studies were performed on an annexin V variant containing a mutation of glutamic acid–95 to serine in the center of the pore region. The mutation resulted in a lower single channel conductance for calcium and a strongly increased conductance for sodium and potassium, indicating that glutamic acid–95 is a crucial constituent of the ion selectivity filter. There were only minor differences in the crystal structures of mutant and wild-type annexin V around the mutation site; however, the mutant showed structural differences elsewhere, including the presence of a calcium binding site in domain III unrelated to the mutation. Analysis of the membrane-bound form of annexin V by electron microscopy revealed no differences between the wild type and mutant.

Annexin V belongs to a family of calcium- and phospholipid-binding proteins (*1*) and forms voltage-dependent calcium channels in planar lipid bilayers (*2*). Our analysis of human annexin V by x-ray crystallography (*3*) revealed a hydrophilic pore in the center of the protein that is filled with a chain of water molecules and that we tentatively identified as the ion-conduction pathway (*3*). We introduced a Glu→Ser mutation at amino acid 95, which is located within the pore, and have analyzed the mutant protein for both functional (ion selectivity) and structural changes.

We prepared phospholipid bilayers from liposomes (*4*) in the inside-out configuration of the patch-clamp technique (*5*). Annexin V was added to the bath solution and bound to the bilayers at the tip of the patch pipette. We recorded single channel currents through wild-type annexin V and the Glu→Ser^{95} mutant channels at different pipette potentials with Ca^{2+} in the pipette and Na^+ in the bath solution (Fig. 1, A and B). Although the mutation caused only a slight decrease in Ca^{2+} currents through the protein, the Na^+ currents were strongly increased. In addition, the voltage dependence of the gating kinetics differed for the two channels (*6*).

We next quantified the single channel conductances and the ion selectivity. For the wild-type and Glu→Ser^{95} annexins, respectively, the Ca^{2+} conductances were 29.5 ± 1.6 pS and 22.0 ± 2.2 pS, the Na^+ conductances were 24.7 ± 1.2 pS and 132.5 ± 4.5 pS, and the reversal potentials were −21.0 ± 1.8 mV and +5.9 ± 1.0 mV (Fig. 1C). The calculated permeability ratio (P_{Ca}/P_{Na}) was 3.75 for the wild-type annexin and 0.71 for the mutant, indicating that the mutant channel had lost selectivity for Ca^{2+} versus Na^+ ions. Similar changes were observed for K^+: For the wild-type and the Glu→Ser^{95} annexins, the K^+ conductances increased from 21.2 ± 1.9 pS to 96 ± 12 pS and the reversal potential shifted from −23.2 ± 1.9 mV to +2.1 mV.

Comparison of the crystal structures of wild-type annexin (*3*) and the Glu→Ser^{95} mutant (*7*) revealed only small differences around the mutated residue (Fig. 2A). In the wild-type molecule, Glu^{95} was hydrogen-bonded across the pore to Arg^{271} and His^{267} (*3*) located in module 1 (consisting of domains I and IV), interactions that are absent in the Glu→Ser^{95} mutant. In contrast, the mutated residue Ser^{95} interacted only with Tyr^{91} in module 2 (consisting of domains II and III). That limitation may diminish the steric hindrance for an ion passing through the pore. Both residues are involved in hydrogen bonds to water molecules.

When the Na-Ca gradient in the single channel measurements was reversed, the inward rectification of the ion currents (Fig. 1C) changed to an outward rectification of

Max-Planck-Institut für Biochemie, 82152 Martinsried, Germany.

*To whom correspondence should be addressed.

similar size (6). This behavior would be predicted from the position of the mutated Glu→Ser[95] residue in the center of the ion pathway through the annexin V pore. Although Glu[95] is surrounded by amino acid side chains (Fig. 2, B and C) providing potential Ca^{2+} ligands, a high-affinity Ca^{2+} binding site within the pore is not obvious in the crystal structure. Nevertheless, a low-affinity Ca^{2+} binding site might be formed with Glu[95] as the main ligand.

Important structural differences in the Glu→Ser[95] mutant were the smaller angle between the two modules and, surprisingly, a Ca^{2+} binding site in domain III (Fig. 2A) that had not been observed in wild-type annexin V (8). The intermodule angle was found to vary in three different wild-type structures (3, 9) and therefore is probably determined by crystal packing. A direct influence of the mutation on the Ca^{2+} binding site could be ruled out because another mutant (Glu→Gln[78]) crystallized in both space groups, the wild-type R3 form and the Glu→Ser[95] R3 form (10). The Glu→Gln[78] mutant had the Ca^{2+} binding site only in the latter.

The Ca^{2+} binding site in domain III was not identical to the Ca^{2+} binding sites identified in domains I, II, and IV. However, the metal was similarly coordinated in a distorted pentagonal bipyramid with an average Ca^{2+}-to-oxygen distance of 2.37 Å, and the Ca^{2+} had a low *B* factor (13.2 Å^2). The Ca^{2+} binding site was formed in part by two carbonyl oxygens from Lys[186] and Gly[188] located in a loop with an exposed Trp at position 187. The Trp[187] is stabilized in this location by van der Waals interactions with residues of a symmetry-related molecule and by a hydrogen bond

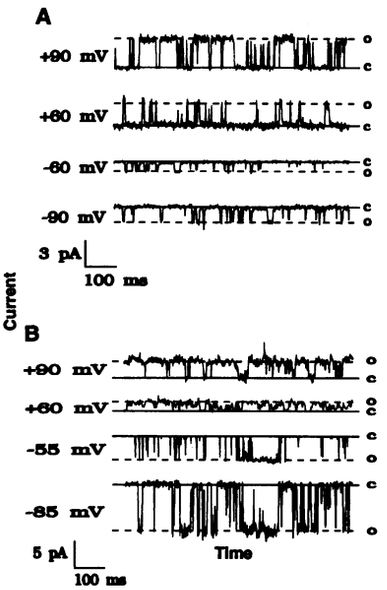

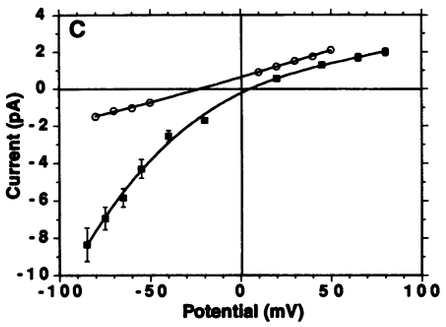

Fig. 1. Single channel current recordings of (**A**) wild-type annexin V and (**B**) the Glu→Ser[95] mutant incorporated into acidic phospholipid bilayers at different pipette potentials (V_p). (**C**) The current-voltage relationships for the wild-type annexin V (open circles) and the Glu→Ser[95] mutant (filled squares) resulting from these current recordings. The continuous lines represent nonlinear least-squares fits.

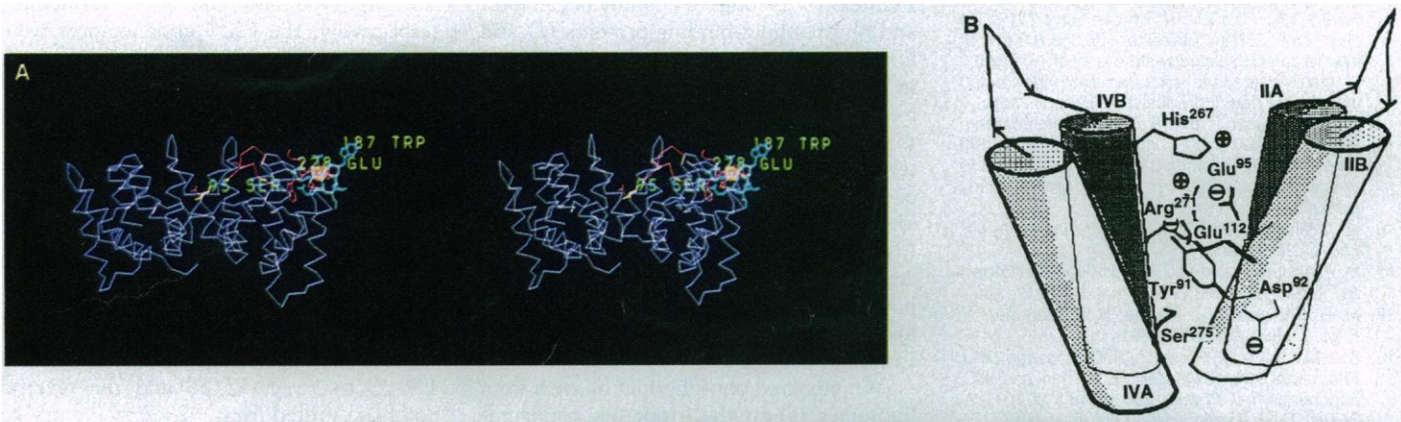

Fig. 2. (**A**) Stereo images showing the Cα trace (purple) of the Glu→Ser[95] mutant. In this side view, the Ca^{2+} binding sites are on the top and the amino terminus is on the bottom. The mutated residue, Glu→Ser[95], is shown in yellow and Glu[95] as found in the wild-type structure (3) is shown in red. The Ca^{2+} binding site in domain III is shown with the loop including Trp[187] and residue Glu[228] in light blue. The calcium ion is represented by the red dotted sphere with the sulfate molecule (light blue) above it. Regions whose conformations differ substantially from that of wild-type annexin V are shown in red (amino acids 225 to 232 with Glu[228] at the top and amino acids 184 to 189 with Trp[187] buried in the core). (**B**) Cylinder representation of the central four-helix bundle forming the hydrophilic pore through annexin V. Potential Ca^{2+}-ligating residues (ionizable groups are marked) are derived from the crystal structure after reasonable side chain rearrangements had been taken into account. The numbering of the helices is as in (3). The polarity of the helices is indicated by arrows. (**C**) Stereo images of the region around the mutated residue. The wild-type structure (red) (3) and the Glu→Ser[95] mutant structure (blue) are overlaid (water molecules are not shown). A $2F_o - F_c$ electron density map (contoured at 0.8 σ; light blue) is overlaid on residue Ser[95]. This residue was omitted for phase calculation. Coordinates of the Glu→Ser[95] mutant annexin have been deposited in the Brookhaven Data Bank.

with a water molecule. The rest of the Ca^{2+} binding site is formed by the carboxylate group of the conserved Glu^{228}, the carbonyl oxygen of Gly^{183}, a water molecule, and a sulfate molecule. In wild-type annexin, the Trp^{187} loop is not exposed but completely buried inside domain III. Another segment of the protein, including the Ca^{2+} ligand Glu^{228}, which lies near the module interface in the wild-type form, was also rearranged in the Glu→Ser^{95} mutant (Fig. 2A). In the presence of calcium, the exposed Trp^{187} in the mutant may penetrate the interface region of the membrane area adjacent to the protein. This hypothesis is supported by the different fluorescence properties of Trp^{187} in the free and membrane-bound forms of annexin V (*11*). The other Ca^{2+} binding sites identified in the wild-type molecule were incompletely occupied in the mutant crystal form.

The conformation of the Trp^{187} loop appears to be dependent on the crystal packing; this observation suggests that there is an energetically delicate balance of conformations whose equilibrium is shifted by calcium. The expulsion of Trp^{187} and its possible penetration of the phospholipid bilayer might occur simultaneously with the electroporation phenomenon probably resulting from the strong electrostatic gradient on the membrane-bound surface of annexin V (*12*), thereby inducing ion channel formation. All synergistic action of these two mechanisms is consistent with the proposal that the phospholipid bilayer becomes ion-permeable after the binding of annexin V without a membrane penetration of the complete molecule.

Several channel-forming proteins undergo structural changes when they bind to membranes (*13*). To investigate the effect of membranes on annexin structure, we prepared two-dimensional crystals of the wild-type protein and the Glu→Ser^{95} mutant on acidic phospholipid monolayers and determined their structures in projection by electron microscopy and image processing (*14*) (Fig. 3, A and B). There were no substantial differences in structure between the mutant and wild-type annexins, and the shape of the membrane-bound form was similar to that determined by x-ray crystallography (Fig. 3C).

The selectivity for Ca^{2+} versus monovalent cations in mutants of the sodium and calcium channels from brain and of the acetylcholine receptor was found to decrease proportionally as the number of positive charges within the putative pore-forming regions was increased (*15*). The Ca^{2+} permeability and the selectivity of glutamate receptors are predominantly controlled by RNA editing, in which the permeability coefficient $P_{divalent}/P_{monovalent}$ is larger when a Gln rather than an Arg occupies the so-called "Gln/Arg site" (*16*). Inspection of the amino acid sequence of annexin VII (*3*), which has a different ion selectivity than annexin V (*17*), reveals that one of the differences in the pore region between the two proteins is the exchange of a Ser residue for the Glu^{95}. Our structure-function analysis leads to the conclusion that amino acid Glu^{95} is an important constituent of the ion pathway and the selectivity filter of annexin V by virtue of its size, charge, and interactions with adjacent amino acid side chains.

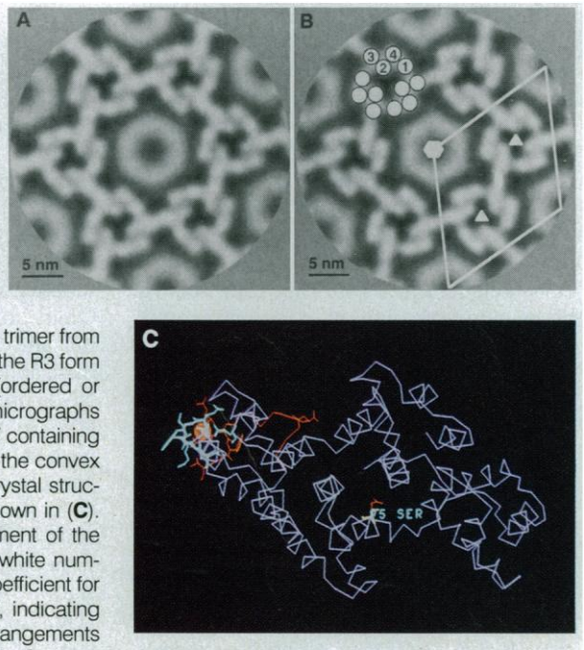

Fig. 3. Electron micrographs of membrane-bound (**A**) wild-type annexin V and (**B**) the Glu→Ser^{95} mutant at 20 Å resolution. The images are views from the membrane side after averaging. The negatively stained crystals are isomorphous, with a p6 lattice and a periodicity of 18.3 nm. The unit cell, outlined by the white diamond in (B), contains two trimers of annexin V and a central ring located on the hexad, which is a translationally and rotationally disordered annexin V trimer. A trimer from the high-resolution crystal structure of the R3 form (*3*) can only be fit into one trimer (ordered or disordered) identified in the electron micrographs when seen from the side of annexin V containing Ca^{2+} binding sites [corresponding to the convex side as in (*3*)]. The high-resolution crystal structure in the described orientation is shown in (**C**). The superposition led to the assignment of the four domains, which are marked by white numbered circles in (B). The correlation coefficient for the two images (A) and (B) is 0.967, indicating that there are no major structural rearrangements at this resolution. (C) Image showing the Cα trace (purple) of the Glu→Ser^{95} mutant, viewed from the convex side. The image includes the mutated residue Glu→Ser^{95} (yellow); residue Glu^{95} (red) as found in the wild-type structure (*3*); and the Ca^{2+} binding site in domain III (amino acids 184 to 189 as found in the wild-type structure are in red and those as found in the mutant structure are in light blue). The calcium ion is shown as a red dotted sphere, and the sulfate is shown in light blue.

REFERENCES AND NOTES

1. M. R. Crompton, S. E. Moss, M. J. Crumpton, *Cell* **55**, 1 (1988); S. E. Moss, Ed., *The Annexins* (Portland Press, London, 1992).
2. E. Rojas, H. B. Pollard, H. T. Haigler, C. Parra, A. L. Burns, *J. Biol. Chem.* **265**, 21207 (1990).
3. R. Huber, J. Römisch, E. Pâques, *EMBO J.* **9**, 3867 (1990); R. Huber, M. Schneider, I. Mayr, J. Römisch, E. Pâques, *FEBS Lett.* **275**, 15 (1990); R. Huber *et al.*, *J. Mol. Biol.* **223**, 683 (1992).
4. Large unilamellar vesicles were formed from phosphatidylserine:phosphatidylethanolamine (molar ratio 9:1) by the dehydration-rehydration technique (*18*). Patches were excised from these liposomes in the inside-out configuration of the patch-clamp technique (*5*). The protein was added to the bath solution at a concentration of 50 nM and bound to the patches in the presence of 1 mM Ca^{2+}. During the current recordings, the pipette solution contained 50 mM $CaCl_2$ and 10 mM Hepes [adjusted to pH 7.4 with tetramethylammonium-hydroxide (TMA)]. The bath solution contained 100 mM NaCl or 100 mM KCl and 10 mM Hepes (pH 7.4 with TMA). The membrane potential across the bilayer was changed by clamping of the pipette potential with respect to the bath. A positive current is defined as net cation flow from the pipette into the bath (positive current is Ca^{2+} current; negative current is Na^{+} current). The currents were sampled at 1 kHz after filtering was done at 3 kHz (−3 dB). The permeability ratio was calculated by the Fatt-Ginsborg voltage equation (*19*).
5. O. P. Hamill, A. Marty, E. Neher, B. Sakmann, F. J. Sigworth, *Pfluegers Arch.* **391**, 85 (1981).
6. R. Berendes, unpublished data.
7. The annexin V complementary DNA was subcloned into the M13mp19 vector, and site-directed mutagenesis was performed as in (*20*). The protein was expressed by means of the pTRC99/A-PP4 vector (*21*), in *Escherichia coli* and purified as in (*22*). The Glu→Ser^{95} mutant was crystallized and harvested as in (*3*). The crystals belonged to space group R3 (cell constants $a = b = 157.5$ Å, $c = 36.4$ Å; $\alpha = \beta = 90°$, $\gamma = 120°$) and were different from the wt R3 form (cell constants $a = b = 99.7$ Å, $c = 96.6$ Å; $\alpha = \beta = 90°$, $\gamma = 120°$). Data were collected on an x-ray imaging plate system (Hendrix/Lantfer, Mar Research, Hamburg). Reflections were integrated with the MOSFLM program (*23*). A formatted reflection file was written to process the data with the CCP4 package, and the data were merged and loaded with the PROTEIN program (*24*). The data collection statistics were as follows: number of observations = 46,563; number of measurements [$I > 0\sigma(I)$] = 30,774; number of independent reflections = 11,143; completeness in ∞ − 2.52 Å = 93.9%, and completeness in 2.71 − 2.52 Å = 93.9%; R_{merge} = 7.9% [$R_{merge} = \Sigma|I(k) - \langle I\rangle|/\Sigma I(k)$, where $I(k)$ and $\langle I\rangle$ are the intensity values of individual measurements and of the corresponding mean values; the summation is over all measurements]; R_f = 3.4% [$R_f = R_{merge}$ after independent averaging of Friedel pairs]. The crystal structure was solved by rotational and translational search techniques (*25*) with the routines as implemented in the X-PLOR program (*26*); the whole wild-type molecule was used as the search model. The structure was further refined by rigid-body minimization as implemented in X-PLOR and then with the conventional least-squares po-

sitional refinement algorithm of X-PLOR (*26*). Between refinement cycles, the structure was inspected on a graphics display with the FRODO program (*27*). The Glu^{95} residue was exchanged with Ser, and segments from amino acids 180 to 190 and 224 to 231 in domain III were manually rebuilt. In later refinement cycles, solvent molecules, calcium, and sulfate were included. The structure was refined with data to 2.52 Å to a final *R* factor of 19.5% ($R = \Sigma||F_o| - |F_c||/\Sigma|F_o|$, where F_o and F_c are the observed and the calculated structure factors, respectively). The refinement statistics were as follows: resolution = 8.0 to 2.52 Å; number of reflections used for refinement = 10,750; total number of non-hydrogen atoms = 2630; protein atoms = 2472; solvent = 151; calcium = 2; sulfate = 1; root-mean-square deviation from target values for bonds = 0.013 Å and for angles = 2.811°; mean B factors for protein atoms = 29.29 $Å^2$ and for solvent = 41.58 $Å^2$.

8. Similar changes have been observed independently by N. O. Concha, J. F. Head, M. A. Kaetzel, J. R. Dedman, and B. A. Seaton [*Science* **261**, 1321 (1993)] and J. Sopkova, M. Renouard, and A. Lewit-Bentley (*J. Mol. Biol.*, in press).
9. A. Lewit-Bentley, S. Morera, R. Huber, G. Bodo, *Eur. J. Biochem.* **210**, 73 (1992).
10. A. Burger, D. Voges, C. Ruiz-Perez, R. Huber, R. Berendes, unpublished data.
11. P. Meers, *Biochemistry* **29**, 3325 (1990); ——— and T. Mealy, *ibid.* **32**, 5411 (1993).
12. A. D. Karshikov *et al.*, *Eur. Biophys. J.* **20**, 337 (1992).
13. M. W. Parker, F. Pattus, A. D. Tucker, D. Tsernoglou, *Nature* **337**, 93 (1989).
14. The crystals on dioleoylphosphatidylserine (DOPS) monolayers were prepared as in (*28*). Eleven microliters of a solution containing 0.6 μM protein, 20 mM tris-HCl (pH 8.4), 100 mM NaCl, and 0.5 mM $CaCl_2$ was placed in teflon wells and covered with 1 μl DOPS [hexane (0.25 mg ml^{-1})]. After 2 hours of incubation at 4°C, the crystals were picked up onto electron microscopy grids covered with perforated carbon film and were negatively stained with uranyl formate. Specimens were observed in a Phillips CM12 electron microscope at an actual magnification of ×33,600 in the low-dose mode. Suitable micrographs were digitized at a pixel size of 15.1 μm. Areas of 0.25 $μm^2$ in real space, corresponding to 600 to 700 unit cells, were averaged according to cross-correlation techniques (*29*).
15. S. H. Heinemann, H. Terlau, W. Stühmer, K. Imoto, S. Numa, *Nature* **356**, 441 (1992); M.-S. Kim, T. Morii, L.-X. Sun, K. Imoto, Y. Mori, *FEBS Lett.* **318**, 145 (1993); A. V. Ferrer-Montiel and M. Montal, *ibid.* **324**, 185 (1993).
16. N. Burnashev, H. Monyer, P. H. Seeburg, B. Sakmann, *Neuron* **8**, 189 (1992); R. Dingledine, R. I. Hume, S. F. Heinemann, *J. Neurosci.* **12**, 4080 (1992); J. Egjeberg and S. F. Heinemann, *Proc. Natl. Acad. Sci. U.S.A.* **90**, 755 (1993).
17. H. B. Pollard and E. Rojas, *Proc. Natl. Acad. Sci. U.S.A.* **85**, 2974 (1988).
18. J. R. Reeves and R. M. Dowben, *J. Cell. Physiol.* **73**, 49 (1969).
19. P. Fatt and B. L. Ginsborg, *J. Physiol. (London)* **142**, 516 (1958).
20. T. A. Kunkel, J. D. Roberts, R. A. Zabour, *Methods Enzymol.* **154**, 367 (1987).
21. E. Amann, B. Ochs, K.-J. Abel, *Gene* **69**, 301 (1988).
22. A. Burger, R. Berendes, D. Voges, R. Huber, P. Demange, *FEBS Lett.* **329**, 25 (1993).
23. A. G. W. Leslie, in *Crystallographic Computing 5*, D. Moras, A. D. Podjarny, J. C. Thierry, Eds. (Oxford Univ. Press, Oxford, 1991), pp. 50–61.
24. W. Steigemann, thesis, Technische Universität, München, Germany (1974).
25. W. Hoppe, *Z. Elektrochem.* **61**, 1076 (1957); M. G. Rossmann and D. M. Blow, *Acta Crystallogr.* **15**, 24 (1962); R. Huber, *ibid.* **19**, 353 (1965).
26. A. T. Brunger, *X-PLOR Manual, Version 2.1* (Yale University, New Haven, 1990).
27. T. A. Jones, *J. Appl. Crystallogr.* **11**, 268 (1978).
28. E. E. Uzgiris and R. D. Kornberg, *Nature* **301**, 125 (1983).
29. W. O. Saxton and W. Baumeister, *J. Microsc.* **127**, 127 (1982).
30. We thank C. Ruiz-Perez for help with the protein crystallization and the data acquisition, A. Cavalié and H. D. Lux for helpful discussions about the electrophysiology, W. Baumeister for access to the electron microscopy facilities, and R. Ficner and P. Reinemer for help with the solution of the crystal structure. Supported by the Deutsche Forschungsgemeinschaft.

21 June 1993; accepted 23 August 1993

Characterization of a Presynaptic Glutamate Receptor

Tania Smirnova, Jacques Stinnakre, Jacques Mallet*

Glutamate receptors mediate excitatory neurotransmission in the brain and are important in the formation of memory and in some neurodegenerative disorders. A complementary DNA clone that encoded a 33-kilodalton protein (GR33) was obtained by screening a library with an antibody generated against glutamate binding proteins. The sequence of GR33 is identical to that of the recently reported presynaptic protein syntaxin. When GR33 was expressed in *Xenopus* oocytes, it formed glutamate-activated ion channels that are pharmacologically similar to those of *N*-methyl-D-aspartate receptors but with different electrophysiological properties. Mutation of the leucine 278 residue in the single putative transmembrane segment of GR33 affects the properties of the channel. Thus, in vivo GR33 may be a presynaptic glutamate receptor.

The family of glutamate-gated ion channels includes receptors activated by *N*-methyl-D-aspartate (NMDA), kainic acid, and α-amino-3-hydroxy-5-methyl-4-isoxazolepropionic acid (AMPA) (*1*). The NMDA receptors have been shown to participate in neuronal plasticity (*1*), long-term potentiation (*2*), and excitotoxicity (*3*) as well as in degenerative disorders (*4*). A large body of evidence indicates that these glutamate receptors are localized postsynaptically. However, recent findings demonstrate that regulation of glutamate release from presynaptic membrane involves one or more presynaptic glutamate autoreceptors (*5*, *6*). Here, we describe the cloning and functional characterization of a new glutamate receptor, which is located presynaptically.

A 1.7-kb fragment of complementary DNA (cDNA), GR33, was obtained from a rat striatal cDNA library with the use of a cDNA clone of 480 base pairs (bp) isolated by immunoscreening of a human cortex library with an antibody generated against glutamate binding proteins (*7*). The amino acid sequence of GR33, which consists of 288 residues, was deduced from the longest open reading frame. A search of the GenBank database revealed that the sequence of the GR33 protein is identical to that of the presynaptic protein syntaxin (p35B) (8) and is similar to a protein of unknown function called HPC-1 (*9*). Syntaxin has been suggested to dock synaptic vesicles near calcium channels at presynaptic active zones (*8*). At its COOH-terminus, this protein has a single hydrophobic region that may be a transmembrane segment (TM).

We tested whether GR33 could function as a glutamate receptor by injecting GR33 complementary RNA (cRNA) into *Xenopus* oocytes (*10*). The GR33 protein formed glutamate-activated channels with a pharmacological profile characteristic of NMDA receptors in several ways (Fig. 1). (i) Application of 100 μM glutamate or 200 μM NMDA evoked inward currents at negative potentials (Fig. 1, A and B) ($n = 32$). The effective dose for half-maximal response (ED_{50}) for NMDA was 10 μM (Fig. 1D), which is similar to data obtained in oocytes injected with either rat brain polyadenylated (*11*) or synthetic NMDA receptor subunit (NMDAR1) mRNAs (*12*). (ii) Omission of glycine from the medium significantly reduced the response to glutamate and to NMDA (Fig. 1, A and B). (iii) NMDA-evoked currents were reduced to 40% in the presence of the competitive NMDA receptor antagonist D-2-amino-7-phosphonoheptanoic acid (10 μM AP7) ($n = 5$) (Fig. 1B), and the responses to glutamate (100 μM) and to NMDA (200 μM) were completely blocked when the concentration of AP7 was increased to 100 μM (Fig. 1, A and B) ($n = 6$). Interestingly, in contrast to the "classic" NMDA receptor, another competitive antagonist, D-2-amino-4-phosphopentanoic acid (AP5; 100 μM), reduced NMDA (200 μM) currents only 40% ($n = 2$); however, AP5 completely blocked responses to glutamate (100

T. Smirnova and J. Mallet, Laboratoire de génétique moléculaire de la neurotransmission et des processus neurodégénératifs, C9923, Centre National de la Recherche Scientifique (CNRS), 91198 Gif sur Yvette, France.
J. Stinnakre, Laboratoire de Neurobiologie Cellulaire et Moléculaire, CNRS, 91198 Gif sur Yvette, France.
*To whom correspondence should be addressed.